

Affinity Space Adaptation for Semantic Segmentation Across Domains

Wei Zhou, Yukang Wang, Jiajia Chu, Jiehua Yang, Xiang Bai, Yongchao Xu

Abstract—Semantic segmentation with dense pixel-wise annotation has achieved excellent performance thanks to deep learning. However, the generalization of semantic segmentation in the wild remains challenging. In this paper, we address the problem of unsupervised domain adaptation (UDA) in semantic segmentation. Motivated by the fact that source and target domain have invariant semantic structures, we propose to exploit such invariance across domains by leveraging co-occurring patterns between pairwise pixels in the output of structured semantic segmentation. This is different from most existing approaches that attempt to adapt domains based on individual pixel-wise information in image, feature, or output level. Specifically, we perform domain adaptation on the affinity relationship between adjacent pixels termed affinity space of source and target domain. To this end, we develop two affinity space adaptation strategies: affinity space cleaning and adversarial affinity space alignment. Extensive experiments demonstrate that the proposed method achieves superior performance against some state-of-the-art methods on several challenging benchmarks for semantic segmentation across domains. The code is available at <https://github.com/idealwei/ASANet>.

Index Terms—Unsupervised domain adaptation (UDA), semantic segmentation, affinity relationship.

I. INTRODUCTION

FOLLOWING the pioneer fully convolutional network (FCN) [1] for semantic segmentation, recent methods [2], [3], [4], [5], [6], [7] have achieved remarkable performances in semantic segmentation using dense pixel-wise annotation. They usually endeavor to boost segmentation accuracy by enlarging receptive fields while preserving fine detail information [4], making use of context information [3], [5], [8], capturing long range dependency via attention mechanism [6], or incorporating structural reasoning via pairwise affinity [2], [7]. Despite these efforts, it is common that a segmentation model trained on a specific domain fails to generalize well on a new one. This is because there exists domain shift between source training images and target testing images. To overcome this, one usually resorts to large amount of pixel-wise labeled target data, which is expensive and tedious to collect. Therefore, semantic segmentation in the wild remains challenging.

Unsupervised domain adaptation (UDA) approaches have been recently studied to address the above issue, where only

W. Zhou, and Y. Xu are with the School of Computer Science, Wuhan University, Wuhan, 430072, China. W. Zhou, Y. Wang, J. Chu, J. Yang, X. Bai, and Y. Xu are with the School of Electronic Information and Communications, Huazhong University of Science and Technology, Wuhan 430074, China (e-mail: weizhou@hust.edu.cn; wangyk@hust.edu.cn; jiajia_chuvip@hust.edu.cn; jiehuayang@hust.edu.cn; xbai@hust.edu.cn; yongchao.xu@whu.edu.cn). (corresponding author: Yongchao Xu.)

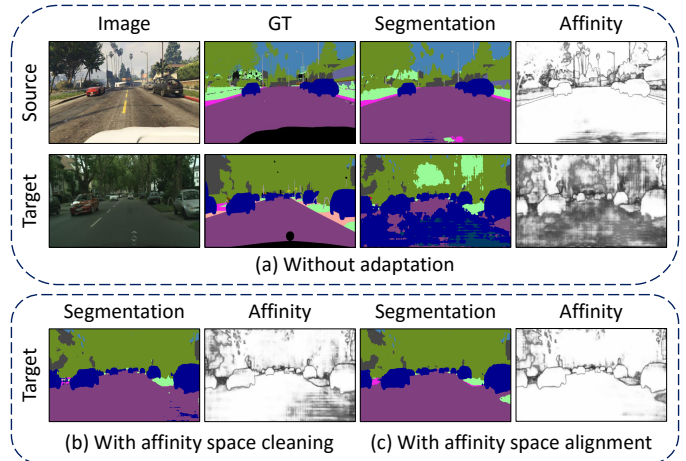


Fig. 1. Proposed affinity space adaptation motivated by similar output structure across domains. We propose to match the affinity space revealing output structure between source and target domain. (a) shows the segmentation results of source and target domain without adaptation. (b) and (c) show the corresponding segmentation results with the proposed affinity space cleaning (ASC) and affinity space alignment (ASA) strategy for affinity space adaptation. For affinity visualization, we show the average Cosine similarity between predictions of each pixel and all its adjacent pixels.

annotations of source domain are provided, but not for the target domain. Such UDA problem has been extensively exploited for image classification, where most prior works attempt to match source and target distributions to learn domain-invariant features by adversarial learning [9]. Similarly, in the field of semantic segmentation, most recent approaches seek to bridge domain gaps by minimizing the difference between the distributions of image style [10], intermediate features [11], [12], [13], or network output space [14]. These existing methods suggest that alignment in image, feature, and output level plays an important role in cross-domain semantic segmentation.

Considering that semantic segmentation is a structured prediction problem, which is robust across domains, it is reasonable to hypothesize that structural knowledge would be beneficial for semantic segmentation across domains. The affinity relationship between output of neighboring pixels contains rich information about spatial structure and local context, which reveals the structural knowledge. Therefore, we introduce the concept of affinity space built upon the affinity relationship between prediction output of each pixel and all its adjacent pixels. We aim to conduct domain adaptation for semantic segmentation on top of this concept. Specifically, we explore two implementations of such concept related to two schemes in different perspectives to achieve such affinity

space adaptation. Firstly, we design an affinity loss that forces high affinity everywhere in the affinity space of both target and source images in addition to segmentation loss on the source domain. Since an image (in both source and target domain) is a priori composed of some continuous semantic regions. Adjacent pixels belonging to the same semantics are dominant over adjacent pixels lying on two different semantic regions. Therefore, such designed affinity loss acts as affinity space cleaning that regularizes the affinity space and results in an affinity space with high value almost everywhere for the target domain, approaching that of source domain. Indeed, as depicted in Fig. 1(a), without adaptation, the affinity space of the target domain is not clean in the sense that there are many low affinities. The proposed affinity space cleaning (see Fig. 1(b)) yields clean and similar affinity maps for the source and target domain. Secondly, we also investigate adversarial training to directly align affinity space distribution of the target domain and that of the source domain. As depicted in Fig. 1(c), adversarial affinity space adaptation also effectively aligns the affinity space.

In summary, the main contributions of this paper are three-fold: 1) We introduce the concept of affinity space that highlights structure through leveraging co-occurring output patterns between neighboring pixels for domain adaptation in semantic segmentation; 2) We propose two effective schemes for affinity space adaptation: affinity space cleaning via affinity loss and adversarial affinity space alignment; 3) The proposed affinity space adaptation achieves superior performance over some state-of-the-art methods on several challenging benchmarks for semantic segmentation across domains.

The rest of this paper is organized as follows. We shortly review some related works in Section II, followed by the proposed method in Section III. Section IV presents extensive experimental results. Finally, we conclude and give some perspectives in Section V.

II. RELATED WORK

We first review some representative works on semantic segmentation in Section II-A, followed by some related works that also leverage pairwise affinity in Section II-B. We then shortly review some recent domain adaptation methods for semantic segmentation across domains in Section II-C. The comparison of the proposed method with some related works is given in Section II-D.

A. Semantic segmentation.

Semantic segmentation is a fundamental task in computer vision. The goal is to assign a category label to each pixel of the image. Driven by the power of deep neural networks, semantic segmentation has achieved great progress since pioneer works: FCN [1] and U-Net [15].

Numerous methods have then been proposed to boost segmentation performance. For example, Deeplab [4], [16] shows that enlarging receptive fields through dilated convolutions leads to significant performance gain. Exploiting context information through atrous spatial pyramid pooling (ASPP) [4], [16], pyramid spatial pooling (PSP) [3] or context

encoding [5] also improve the segmentation accuracy. Some other methods [2], [17], [7] attempt to incorporate pairwise relation to provide structured reasoning that helps to alleviate inconsistency issue in semantic segmentation. Recently, DANet [18] and OCNet [19] propose to utilize self-attention mechanism to capture long range dependency and achieve superior performances.

These fully supervised methods rely on large amount of pixel-wise annotated data. However, it is claimed in [20] that experts spend up to 90 minutes per image for pixel-wise annotation. Some weakly supervised approaches are proposed to leverage easy-attained annotations like image level label [21], [22], bounding boxes [23], [24] or scribbles [25] to circumvent the expensive cost of pixel-wise annotations. Another direction addressing the annotation problem is to leverage synthetic datasets, *e.g.*, GTA5 [20] and SYNTHIA [26]. Though synthetic data with annotations is rather easy to collect, the performance of models trained on synthetic data drops drastically when applied on real scene due to the domain shift between synthetic and realistic data.

B. Pairwise affinity.

Pairwise pixel affinity has a long history use in computer vision tasks. In early vision [27], local affinity has been utilized to characterize the intrinsic geometric structure. Pairwise affinity has been involved in segmentation as clustering cues in [28], [29]. Recently, pairwise pixel affinity has been combined with convolutional neural network (CNN) to provide structure reasoning for semantic or instance segmentation. Example works are [4], [2], [7], [17], [30]. In [4], [2], the authors leverage pairwise affinity via conditional random field (CRF). An adaptive loss built on affinity is proposed in [7] to improve segmentation accuracy. In [17], the authors propose spatial propagation networks to learn affinity for improving semantic segmentation. In [30], the authors explicitly regress pairwise affinity, serving to separate instances of the same semantic for instance segmentation.

C. Domain adaptation

Domain adaptation aims to address the domain-shift problem between the source and target domains. Numerous methods [31], [32], [33], [34], [35], [36], [37], [38] are developed for image classification across domains. The main idea is to minimize the difference of distributions across domains by adversarial learning.

Similar to adaptation on classification, most modern adaptation models for semantic segmentation also rely on adversarial learning to adapt domains either in intermediate feature level [11], [39], [40], [41] or output level [14], [42], [43]. UDA for semantic segmentation was firstly addressed in [11] that aligns the global features of source and target domains via adversarial network. Recently, in [41], a significance-aware information bottleneck is introduced to align domains in latent feature space. It has been shown in [14], [42], [43], [44] that aligning domains in output level may be a better choice than feature level for semantic segmentation across domains. In [14], the authors first propose to explicitly align domains on

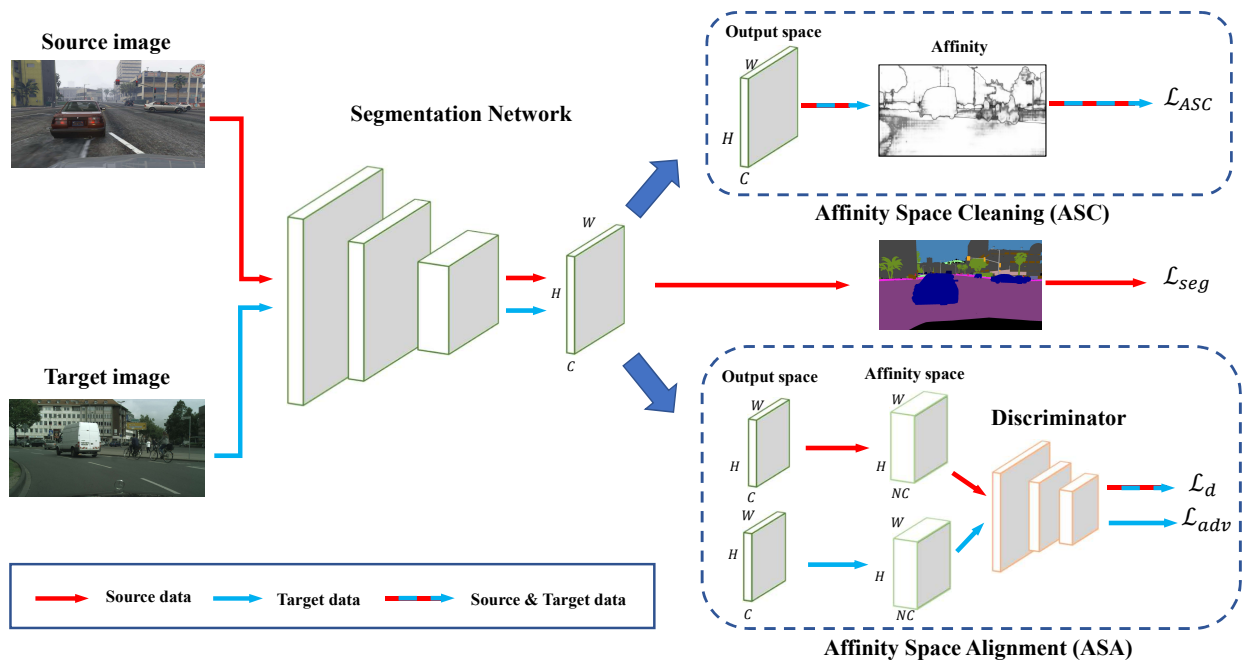


Fig. 2. Overview of the proposed approach. For affinity space adaptation with affinity space cleaning, an affinity-based loss \mathcal{L}_{ASC} is imposed on both source and target domain. For adversarial affinity space alignment strategy, we utilize adversarial training to make affinity space look similar across domains. Red arrows are used for source domain, blue arrows are used for target domain and the mixed arrows represent both domains. For both affinity space adaptation schemes, a segmentation loss \mathcal{L}_{seg} is also computed between segmentation predictions and provided annotations on source images.

the structured output, which is then improved or extended by introducing new loss functions [42], [43] or extra patch-level output space alignment [44].

In addition to the distribution (*i.e.*, feature or output level) alignment strategies that regard each semantic category equally, some approaches [45], [46], [44] tend to boost the performance for some specific categories or regions. In [45], Luo *et al.* propose a category-level adversarial network which adaptively weights the adversarial loss for category-level adaptation. SSF-DAN [46] utilizes pseudo labels to get semantic features of each class for separated adaptation, which brings performance gain on less frequent classes. In [44], Tsai *et al.* take multi modes of patch-wise output distribution into consideration and attach an additional patch alignment module to [14], further improving the adaptation performance. These recent methods suggest that class- or region-conditioned adaptation is beneficial for semantic segmentation across domains based on distribution alignment.

Techniques like image translation and self-training have been proved useful or complementary to the distribution alignment based methods for domain adaptation in many works [10], [47], [48], [49], [50], [44]. In [10], the authors utilize CycleGAN [51] to generate extra target data in addition to adversarial adaptation on the feature level. DCAN [47] performs image-level and feature-level adaptation at the same time. DISE [49] disentangles images into domain-invariant structure and domain-specific textures for better image translation and label transfer. In CBST [48], the authors propose a novel class-balanced self-training framework, where imbalanced class distribution and spatial priors are taken into consideration. More recently, BDL [50] proposes a bidirectional

learning framework to make the image translation model, the segmentation adaptation model, and self-training model learn alternatively, further boosting the performance.

Some other methods seek to reduce domain gap via effective utilization of source data [52], designing loss function [53], [43], curriculum model adaptation [54], [55], or self-ensembling strategy [56], [57]

D. Comparison with related works

Most existing approaches for unsupervised domain adaptation focus on aligning domains based on individual pixel-wise information in image, intermediate feature, or output level. Though these approaches have achieved remarkable performance across domains, the structural and contextual representation is not explicitly exploited. We propose to highlight structure through leveraging co-occurring patterns between pairwise pixels in the output level of structured semantic segmentation. The proposed approach performs domain adaptation on the affinity space given by the affinity relationship between adjacent pixels in the output prediction. We exploit two affinity space adaptation strategies: affinity space cleaning and adversarial affinity space alignment. Though the proposed method is driven by the importance of pairwise affinity involved in some fully supervised segmentation methods, we leverage the pairwise affinity in a different way by constructing an affinity space and performing domain adaptation on it. This demonstrates for the first time that the affinity relationship is beneficial for UDA in semantic segmentation.

III. APPROACH

A. Overview

Given the source data $\mathbb{X}_S \subset \mathbb{R}^{H \times W \times 3}$ with dense pixel-wise annotations $\mathbb{Y}_S \subset (1, \dots, C)^{H \times W}$ and the target data $\mathbb{X}_T \subset \mathbb{R}^{H \times W \times 3}$ without annotations. Unsupervised domain adaptation (UDA) in semantic segmentation aims to train a model that performs well on the target data \mathbb{X}_T , where H and W is the image height and width, respectively, and C is the number of classes. Considering that the semantic segmentation is a structured prediction problem, we leverage the pairwise co-occurring patterns that reveals the output structure being invariant across domains. Specifically, we introduce the concept of affinity space which is built upon affinity between adjacent pixels in the output space. We perform UDA for semantic segmentation on the affinity space instead of on information (from image, feature, or output level) of individual pixel. To this end, we propose two schemes to adapt based on the concept of affinity space, which describes the similarity between adjacent pixels and has different implementations depending on the proposed schemes. The first strategy implicitly regularizes the affinity space via an affinity space cleaning loss (see Section III-B). The second one is an adversarial framework that explicitly aligns affinity distribution across domains (see Section III-C). The pipeline of the proposed affinity space adaptation framework is illustrated in Fig. 2. The adopted network architecture for performing the semantic segmentation across domains is depicted in Section III-D.

B. Affinity space cleaning

The semantic segmentation can be regarded as a structured prediction problem. Even though there is no ground-truth for the target images, we may still impose some constraints on the output structures. Indeed, based on the observation (see Fig. 1) about affinity between adjacent pixels in the output space, we notice that the affinity is unclean in the sense that it is low on most part of target images without adaptation. For an expected semantic segmentation, the affinity is low only on edges of adjacent semantic regions, resulting in a clean affinity map. Therefore, we propose an affinity space cleaning loss on both source and target images to force the network to produce clean affinity map of output space. For an image X , the proposed affinity space cleaning (ASC) loss is formulated as following:

$$\mathcal{L}_{ASC}(X) = \frac{1}{|X|} \sum_{x \in X} \sum_{n \in \mathcal{N}(x)} 1 - \frac{P_x \cdot P_n}{\|P_x\| \|P_n\|}, \quad (1)$$

where $\mathcal{N}(x)$ is the set of 4 or 8 spatially adjacent neighbors of pixel x , $|\cdot|$ denotes the cardinality, P stands for the Softmax output prediction, and $\|\cdot\|$ is the magnitude of the vector. Minimizing such affinity space cleaning loss encourages high affinity everywhere. Though such ASC on border pixels does not entirely make sense, in most cases, pairwise adjacent pixels lying on the same semantic region dominate over adjacent pixels from two different semantic regions in the expected segmentation. Incorporating the structure reasoning in this way is reasonable and regularizes the affinity space of the target

domain to approach that of the source domain. For a target image X_t , we minimize such affinity cleaning loss. For a source image X_s with ground-truth annotation Y_s , we also optimize the following cross-entropy loss for segmentation:

$$\mathcal{L}_{seg}(X_s) = -\frac{1}{|X_s|} \sum_{h,w} \sum_{c \in C} Y_s^{(h,w,c)} \log(P_s^{(h,w,c)}), \quad (2)$$

where Y_s is the one-hot representation of ground-truth annotation. The final objective function to be minimized for this affinity space adaptation scheme is given by:

$$\mathcal{L} = \mathcal{L}_{seg}(X_s) + \lambda_{ASC} \mathcal{L}_{ASC}(X_s) + \lambda_{ASC} \mathcal{L}_{ASC}(X_t), \quad (3)$$

where λ_{ASC} is a weighting factor (set to a small value, *e.g.*, 0.001) that represents the importance of loss \mathcal{L}_{ASC} . The ASC loss in Eq. (1) acts somehow as smoothing the region in target images without supervision, and is in the range of [0, 1]. In the beginning of training when the target prediction is not accurate, the cross-entropy loss for segmentation $\mathcal{L}_{seg}(X_s)$ on the source images is much larger than $\lambda_{ASC} = 0.001$. Thus, the beginning of training is mainly guided by the segmentation loss on the source images. When the segmentation loss on the source image drops to a relatively small value, the segmentation model already possesses a certain ability in segmenting the target images, and the ASC begins to influence the network training. Therefore, the proposed ASC strategy in general does not harm the model training.

Another interpretation of the proposed ASC may be that by optimizing on the source images in a fully supervised way, the segmentation model already possesses a certain ability in predicting semantic labels on target images. By further minimizing \mathcal{L}_{ASC} , we enforce the adjacent pixels to have the same label prediction, which can somehow propagate accurate classification score from current pixel to nearby pixels belonging to the same semantic region.

C. Affinity space alignment

We also propose an adversarial framework to explicitly align the affinity space distribution of the target domain to that of the source domain. In this way, we could transfer knowledge of co-occurring patterns from the source domain to the target domain, *e.g.* the sky class is always on the top of the building class and the rider class always comes up with bike or motorcycle class. For such adversarial affinity space alignment (ASA), we begin with constructing the affinity space $A \in \mathbb{R}^{H \times W \times NC}$ from the output prediction $P \in \mathbb{R}^{H \times W \times C}$, where N (4 or 8 for 4-connectivity or 8-connectivity) is the number of involved adjacent pixels on each pixel. Precisely, for a pixel x and one of its neighboring pixel n , we denote $P_x = (p_x^1, \dots, p_x^C)$ and $P_n = (p_n^1, \dots, p_n^C)$ as the corresponding C -class Softmax output vector. We then build the affinity space A based on affinity related vector $A_n = (a_n^1, \dots, a_n^C)$ using KL divergence-like measure on each class, where $a_n^i = (p_x^i \log(\frac{p_x^i}{p_n^i}) + (1 - p_x^i) \log(\frac{1 - p_x^i}{1 - p_n^i}))$ for i -th class. For N pairs of neighboring pixels of underlying pixel x , we have N such affinity vectors, resulting in a vector of NC channels by concatenating them together $A = (A_1, \dots, A_N)$. This gives rise to an affinity space

A of size $H \times W \times NC$ for each image X . Such KL divergence-like measure on each class preserves better the co-occurring information between different classes than K-way KL divergence and Cosine similarity which squeeze all channels into a scalar similarity between neighboring pixels. For example, adjacent pixels of different K-way classification probability may result in the same value for these scalar measurements. With the proposed KL divergence-like measure on each class, different vectors are produced.

Given an image X from the source domain or target domain, the segmentation network produces an affinity space A . We forward the affinity space A to a fully-convolutional discriminator D using a binary cross-entropy loss \mathcal{L}_d for the source and target domains. The loss \mathcal{L}_d is formulated as:

$$\mathcal{L}_d(A) = - \sum_{h,w} ((1-z)\log(D(A)^{(h,w,0)}) + z\log(D(A)^{(h,w,1)})), \quad (4)$$

where z equals 0 for sample from target domain, and z is 1 for sample from the source domain. For an image X_t from the target domain, the adversarial objective to train the segmentation network is given by:

$$\mathcal{L}_{adv}(A_t) = - \sum_{h,w} \log(D(A_t)^{(h,w,1)}). \quad (5)$$

The goal is to train the segmentation network and fool the discriminator by maximizing the probability of affinity space A_t of the target domain being considered as the affinity space of the source domain. Collaborating with the segmentation loss in Eq. (2) on source images, the overall loss function to train the segmentation network can be written as:

$$\mathcal{L}_{ASA}(X_s, X_t) = \mathcal{L}_{seg}(X_s) + \lambda_{ASA}\mathcal{L}_{adv}(A_t), \quad (6)$$

where λ_{ASA} is the weighting factor for the adversarial term \mathcal{L}_{adv} . During training, we alternatively optimize discriminator network D and the segmentation network using loss function in Eq. (4) and Eq. (6), respectively.

D. Network architecture

For the semantic segmentation network, we adopt the same network architecture as [14]. More specifically, we adopt Deeplab-V2 model [4] as the base architecture while discarding the multi-scale fusion strategy. We evaluate the proposed method with two CNN backbones: VGG-16 [58] and ResNet-101 [59], both of which are initialized with the model pre-trained on ImageNet [60]. Following [4], we modify the stride and dilation rate of the last two convolutional layers of CNN backbones. Atrous Spatial Pyramid Pooling (ASPP) with dilation rates $\{6, 12, 18, 24\}$ is also applied on the last layer of both backbone models. For the discriminator, we choose the similar network architecture used in [14] for the proposed adversarial affinity space alignment. More precisely, the discriminator is composed of five 4×4 convolution layers with stride 2 and channel numbers $\{64, 128, 256, 512, 1\}$, respectively. Each convolutional layer, except the last one, is followed by a leaky-ReLU layer with a fixed negative slope of 0.2.

IV. EXPERIMENTS

To validate the effectiveness of the proposed approach for semantic segmentation across domains, we conduct experiments on two popular domain adaptation benchmarks: GTA5 [20] to Cityscapes [61] and SYNTHIA [26] to Cityscapes. Experimental results, including cross-city case and medical image segmentation across domains, are also given for validation on real-to-real adaptation scenarios. In the following, we clarify the implementation details and compare the proposed method with other state-of-the-art approaches using similar backbones.

A. Datasets & evaluation metrics

Synthetic-to-Real adaptation. We first conduct experiments on synthetic-to-real adaptation using Cityscapes [61] as the target dataset, GTA5 [20] and SYNTHIA [26] as the source dataset, respectively. The details about these datasets are shortly described as follows.

Cityscapes [61] is a widely used dataset for semantic segmentation, which contains high-quality dense annotations of 5000 images collected from 50 cities. The dataset is divided into 2975, 500, and 1525 images for training, validation, and testing, respectively. It provides 30 common classes, of which 19 classes are used for evaluation.

GTA5 [20] is a synthetic dataset containing 24966 images built with the gaming engine Grand Theft Auto V. Pixel-level semantic annotations of 33 classes are provided. Following other methods, we only use the common 19 classes to pair with the Cityscapes [61] dataset.

SYNTHIA [26] is another large synthetic dataset rendered by the Unity game engine. Its subset, named SYNTHIA-RAND-CITYSCAPES, provides 9400 images with labels compatible with the Cityscapes [61] classes. Different from GTA5, this dataset contains synthetic images with various viewpoints, making it challenging for domain adaptation.

Following previous works [48], [14], [42], we utilize labeled synthetic images and unlabeled training images of Cityscapes to perform adaptation and evaluate the proposed adapted model on Cityscapes ‘val’ split.

Real-to-Real adaptation. We also evaluate on real-to-real adaptation scenarios to further validate the effectiveness of the proposed method. For that, we conduct experiments on cross-city dataset [62] and two retinal fundus image datasets: REFUGE [63] and RIM-ONE-r3 [64]. The details of these datasets are shortly given in the following.

Cross-city [62] is a high-quality road scene dataset collected from four different cities: Rome, Rio, Tokyo, and Taipei. Each city consists of 3200 unlabeled images and 100 Cityscapes-compatible annotated images. Similar to [62], we adopt the Cityscapes training set as the source domain and adapt the segmentation model to each target city using 3200 unlabelled images. The other 100 annotated images of each dataset are used for evaluation.

REFUGE [63] and *RIM-ONE-r3* [64] are two retinal fundus image datasets for retinal optic disk and cup segmentation.

TABLE I

QUANTITATIVE COMPARISON WITH SOME STATE-OF-THE-ART METHODS ON ADAPTING GTA5 TO CITYSCAPES. IN THE FIRST AND SECOND GROUPS, VGG-16 AND RESNET-101 BACKBONE NETWORKS ARE ADOPTED, RESPECTIVELY. METHODS TRAINED USING MULTI-LEVEL ADAPTATION ARE MARKED WITH †.

GTA5 → Cityscapes																				
Method	road	sidewalk	building	wall	fence	pole	light	sign	veg	terrain	sky	person	rider	car	truck	bus	train	mbike	bike	mIoU
FCNs in the Wild [11]	70.4	32.4	62.1	14.9	5.4	10.9	14.2	2.7	79.2	21.3	64.6	44.1	4.2	70.4	8.0	7.3	0.0	3.5	0.0	27.1
CyCADA [10]	83.5	38.3	76.4	20.6	16.5	22.2	26.2	21.9	80.4	28.7	65.7	49.4	4.2	74.6	16.0	26.6	2.0	8.0	0.0	34.8
AdaptSegNet [14]	87.3	29.8	78.6	21.1	18.2	22.5	21.5	11.0	79.7	29.6	71.3	46.8	6.5	80.1	23.0	26.9	0.0	10.6	0.3	35.0
ADVENT [42]	86.9	28.7	78.7	28.5	25.2	17.1	20.3	10.9	80.0	26.4	70.2	47.1	8.4	81.5	26.0	17.2	18.9	11.7	1.6	36.1
SIBAN [41]	83.4	13.0	77.8	20.4	17.5	24.6	22.8	9.6	81.3	29.6	77.3	42.7	10.9	76.0	22.8	17.9	5.7	14.2	2.0	34.2
Source Only (our)	54.5	15.9	64.5	13.6	19.1	16.9	20.0	6.5	77.3	9.4	74.9	46.3	10.6	47.4	11.2	13.2	0.1	11.6	0.8	27.1
ASC (our)	85.2	7.8	75.5	14.0	22.6	17.8	22.8	10.0	78.2	21.1	59.9	48.3	9.2	79.9	21.2	23.4	0	18.0	0.7	32.4
ASA (our)	86.9	32.5	79.0	22.8	23.1	20.7	22.0	12.6	80.0	32.2	68.5	43.6	11.9	81.3	20.8	9.6	4.2	16.9	8.5	35.6
AdaptSegNet [14]	86.5	25.9	79.8	22.1	20.0	23.6	33.1	21.8	81.8	25.9	75.9	57.3	26.2	76.3	29.8	32.1	7.2	29.5	32.5	41.4
AdaptSegNet† [14]	86.5	36.0	79.9	23.4	23.3	23.9	35.2	14.8	83.4	33.3	75.6	58.5	27.6	73.7	32.5	35.4	3.9	30.1	28.1	42.4
ADVENT† [42]	89.9	36.5	81.6	29.2	25.2	28.5	32.3	22.4	83.9	34.0	77.1	57.4	27.9	83.7	29.4	39.1	1.5	28.4	23.3	43.8
SIBAN [41]	88.5	35.4	79.5	26.3	24.3	28.5	32.5	18.3	81.2	40.0	76.5	58.1	25.8	82.6	30.3	34.4	3.4	21.6	21.5	42.6
MaxSquare [43]	88.1	27.7	80.8	28.7	19.8	24.9	34.0	17.8	83.6	34.7	76.0	58.6	28.6	84.1	37.8	43.1	7.2	32.2	34.2	44.3
Source Only (our)	84.2	9.4	74.6	14.6	17.9	22.4	27.8	17.8	69.1	12.4	73.0	55.3	27.0	82.6	30.9	37.9	3.2	27.6	35.6	38.1
ASC (our)	85.5	23.8	79.8	18.9	21.1	27.5	36.6	18.8	82.7	25.9	76.0	59.7	29.0	81.7	33.1	43.5	14.1	33.7	41.4	43.8
ASA (our)	89.2	27.8	81.3	25.3	22.7	28.7	36.5	19.6	83.8	31.4	77.1	59.2	29.8	84.3	33.2	45.6	16.9	34.5	30.8	45.1

REFUGE [63] has 400 high resolution training images. RIM-ONE-R3 [64] dataset contains 99 training samples and 60 samples for testing. Both datasets have precise pixel-wise segmentation annotations for optic disk and cup. We use the 400 high resolution training images in REFUGE [63] as the source domain, and adapt the segmentation model to 99 samples of the RIM-ONE-R3 [64] dataset. We report segmentation results on the 60 test images in RIM-ONE-R3 [64] dataset.

Evaluation metric. In all experiments, we adopt the widely used Intersection-over-Union (IoU) for both synthetic-to-real and real-to-real segmentation adaptation on road scenes and Dice coefficients (DSC) for segmentation adaptation on medical images. Concretely, the two evaluation metrics are given by:

$$IoU = \frac{TP}{TP + FP + FN}, \quad (7)$$

$$DSC = \frac{2TP}{2TP + FP + FN}, \quad (8)$$

where TP , FP , and FN represent the number of true positive, false positive, and false negative pixels, respectively.

B. Implementation details

The implementation is based on the public toolbox PyTorch [65]. All experiments are performed on a workstation with an NVIDIA TITAN Xp GPU card of 12GB memory. For a fair comparison, we use the same hyper-parameter settings with AdaptSegNet [14]. More specifically, for the segmentation model, we use SGD as the optimizer with “poly” learning rate policy where the learning rate equals to $base_lr * (1 - \frac{iter}{total_iter})^{power}$. We set the initial learning rate $base_lr$ to 2.5×10^{-4} and the $power$ to 0.9. The momentum is set to 0.9 and the weight decay is set to 0.0005. For the discriminator, we employ Adam optimizer with an initial learning rate 1×10^{-4} . The momentum is set as 0.9 and 0.99. The hyper-parameter λ_{ASC} in Eq. (3), and λ_{ASA} in Eq. (6)

are all set to 0.001 for all experiments in this paper. Except explicitly stated, we use 8-connectivity adjacent pixels to define affinity space. Due to limited GPU memory, during training, the GTA5 (*resp.* SYNTHIA) source images are resized to 720×1280 (*resp.* 760×1280), and the target Cityscapes images are resized to 512×1024 for all experiments. In the testing phase, the same size 512×1024 as the training phase for Cityscapes is used. The segmentation result is then resized to the original input size at evaluation time. In the real-to-real adaptation experiments, we resize the images into 512×1024 as the training input for cross-city adaptation, and the images are resized to 512×512 on both REFUGE and RIM-ONE-r3 dataset for segmentation adaptation on medical images. Note that we do not use the ground truth to select the best adapted model. Instead, as we hypothesize in Section III-B, an expected semantic segmentation network produces clean affinity of output space. Thus, we select the the adapted model by calculating the average pixel affinity on the train set (ground-truth-free). Specifically, we select the model which has the largest average pixel affinity value over the train set of the target domain.

C. Synthetic-to-real adaptation results

The proposed method aims to perform adaptation by aligning affinity space of output prediction and thus falls into the category of distribution alignment (DA) based methods. Therefore, we first compare the proposed approach with some state-of-the-art methods attempting to leverage adversarial training to align feature or output distributions. We then explore the complementary of the proposed approach with image translation (IT) and self-training (ST) using pseudo labels, and compare with some related approaches which also make use of these techniques. Note that The related methods that use a different backbone network other than VGG16 or ResNet101 are not compared in this paper.

Comparison with related DA-based approaches. We first compare the proposed method with some related distribution

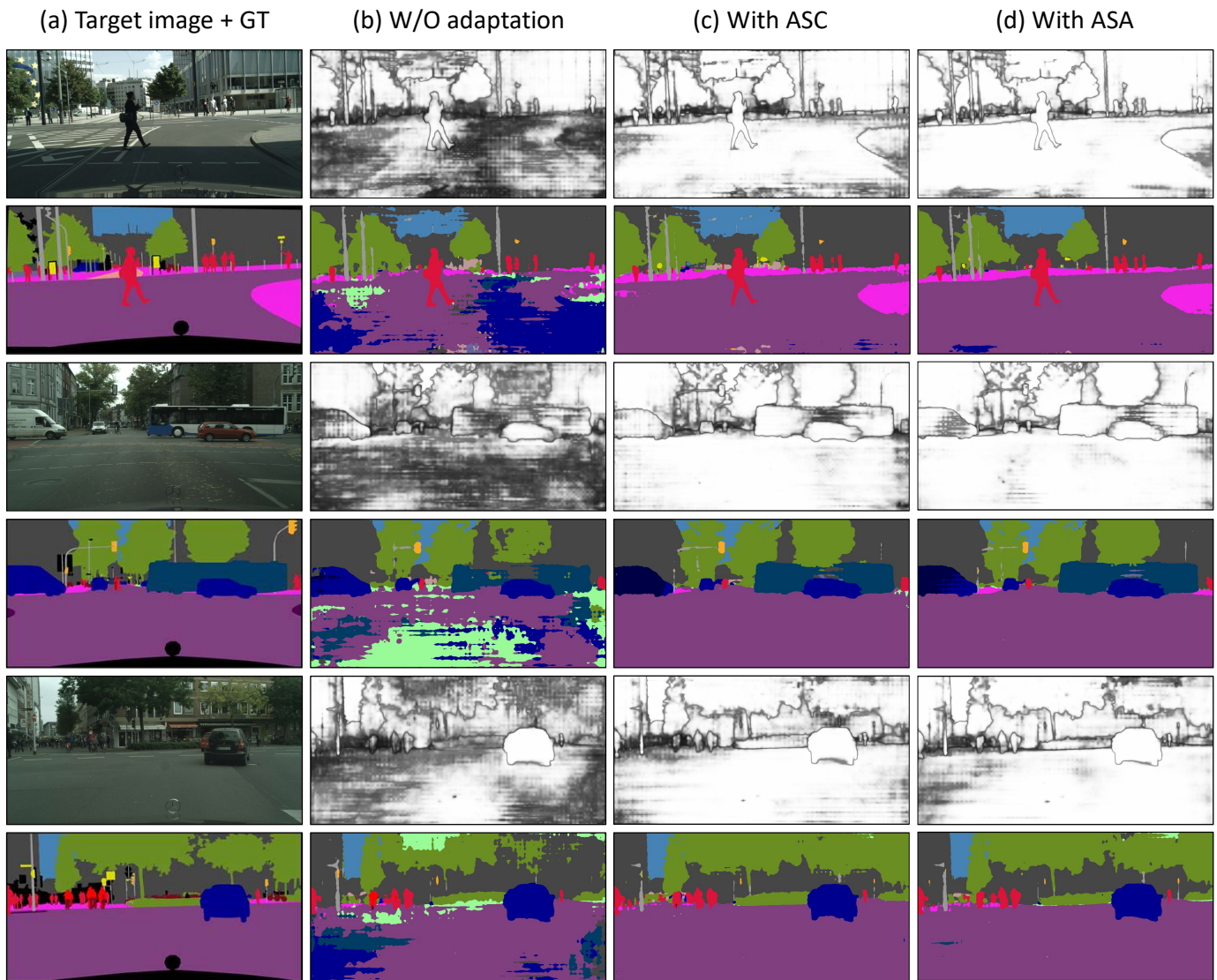


Fig. 3. Qualitative results on GTA5 \rightarrow Cityscapes adaptation. (a) Target images and the corresponding GTs. (b-d): affinity map and semantic segmentation results before adaptation in (b), using proposed affinity space cleaning in (c), and with proposed adversarial affinity space alignment in (d).

alignment (DA) based approaches. The methods relying on class- or region-conditioned adaptation to boost the performance for some specific categories or regions, are not included in the comparison.

GTA5 \rightarrow Cityscapes. We first benchmark the proposed method on adapting GTA5 to Cityscapes. Tab. I depicts the performance comparison with several state-of-the-art methods. The proposed affinity space adaptation achieves competitive or superior performance. Specifically, the proposed affinity space cleaning performs competitively with other methods using both VGG16 and ResNet101 backbones. Using ResNet101 backbone, the proposed ASC yields 43.8% mIoU, outperforming multi-level setting of [14] by 1.4% and similar single-level setting of [14] by 2.4% in terms of mIoU. It is also noteworthy that the proposed ASC with the designed affinity loss does not rely on additional adversarial discriminator, leading to more efficient training. The proposed adversarial affinity space alignment further boosts the performance for

both VGG16 and ResNet101 backbones. More precisely, the proposed ASA using ResNet101 backbone outperforms recent works which directly aligns the Softmax output [14] or output entropy [42] between the source domain and the target domain (under multi-level adaptation) by 2.7% and 1.3% mIoU, respectively. Compared with SIBAN [41] and MaxSquare [43], the proposed ASA records an improvement of 2.5% mIoU and 0.8% mIoU, respectively. Some qualitative results of the proposed affinity space adaptation are given in Fig. 3. The proposed method effectively aligns the affinity space, resulting in adapted semantic segmentation across domains.

SYNTHIA \rightarrow Cityscapes. We then benchmark the proposed method on adapting from SYNTHIA dataset to Cityscapes. Following prior works [14], [42], we report both 16 and 13-categories (marked with *) results in Tab. II. The same observation also holds as on the GTA5 to Cityscapes adaptation. The proposed ASC achieves results on par with several state-of-the-art methods. Consistent to the results of adaptation from GTA5

TABLE II

QUANTITATIVE COMPARISON WITH SOME STATE-OF-THE-ART METHODS ON ADAPTING SYNTHIA TO CITYSCAPES. IN THE FIRST AND SECOND GROUPS, VGG-16 AND RESNET-101 BACKBONE NETWORKS ARE ADOPTED, RESPECTIVELY. METHODS TRAINED USING MULTI-LEVEL ADAPTATION ARE MARKED WITH †.

SYNTHIA → Cityscapes																			
Method	road	sidewalk	building	wall	fence	pole	light	sign	veg	sky	person	rider	car	bus	mbike	bike	mIoU	mIoU*	
FCNs in the wild [11]	11.5	19.6	30.8	4.4	0.0	20.3	0.1	11.7	42.3	68.7	51.2	3.8	54.0	3.2	0.2	0.6	20.2	22.1	
AdaptSegNet [14]	78.9	29.2	75.5	-	-	-	0.1	4.8	72.6	76.7	43.4	8.8	71.1	16.0	3.6	8.4	-	37.6	
ADVENT [42]	67.9	29.4	71.9	6.3	0.3	19.9	0.6	2.6	74.9	74.9	35.4	9.6	67.8	21.4	4.1	15.5	31.4	36.6	
SIBAN [41]	70.1	25.7	80.9	-	-	-	3.8	7.2	72.3	80.5	43.3	5.0	73.3	16.0	1.7	3.6	-	37.2	
Source Only (our)	3.13	11.9	63.7	7.0	0.2	21.1	3.4	10.3	71.0	75.6	46.6	4.4	57.5	18.8	2.1	4.4	25.1	28.7	
ASC (our)	6.1	11.9	76.0	2.4	0.2	20.6	7.5	13.6	76.9	75.7	50.7	12.5	70.0	21.5	3.1	8.0	28.5	33.3	
ASA (our)	72.6	24.2	74.2	8.6	0.6	21.3	6.1	12.6	73.7	77.0	42.3	13.0	67.9	19.1	6.0	14.3	33.3	38.7	
AdaptSegNet [14]	79.2	37.2	78.8	-	-	-	9.9	10.5	78.2	80.5	53.5	19.6	67.0	29.5	21.6	31.3	-	45.9	
AdaptSegNet† [14]	84.3	42.7	77.5	9.3	0.2	22.9	4.7	7.0	77.9	82.5	54.3	21.0	72.3	32.2	18.9	32.3	40.0	46.7	
ADVENT† [42]	87.0	44.1	79.7	9.6	0.6	24.3	4.8	7.2	80.1	83.6	56.4	23.7	72.7	32.6	12.8	33.7	40.8	47.6	
SIBAN [41]	82.5	24.0	79.4	-	-	-	16.5	12.7	79.2	82.8	58.3	18.0	79.3	25.3	17.6	25.9	-	46.3	
MaxSquare [43]	77.4	34.0	78.7	5.6	0.2	27.7	5.8	9.8	80.7	83.2	58.5	20.5	74.1	32.1	11.0	29.9	39.3	45.8	
Source Only (our)	54.8	23.1	73.7	8.5	0.1	25.4	10.5	10.3	74.7	80.1	54.8	16.3	42.3	27.7	20.9	19.1	33.9	39.1	
ASC (our)	77.6	31.2	75.1	4.3	0.2	26.5	9.7	10.9	78.9	81.6	55.2	19.6	76.4	26.1	16.9	29.3	38.7	45.3	
ASA (our)	91.2	48.5	80.4	3.7	0.3	21.7	5.5	5.2	79.5	83.6	56.4	21.0	80.3	36.2	20.0	32.9	41.7	49.3	

to Cityscapes, the proposed affinity space adaptation with ASA strategy performs competitively with the state-of-the-art methods. Precisely, the proposed ASA using ResNet101 backbone improves multi-level setting of [14] and [42] by 2.6% and 1.7% mIoU, respectively, and outperforms the similar single-level setting of [14] by 3.4% mIoU. Compared with the method in [41] and in [43], the proposed ASA brings 3.0% mIoU and 3.5% mIoU improvement, respectively. For VGG16 backbone, the proposed ASA achieves 1.1% mIoU improvement against [14]. The improvement of the proposed affinity space adaptation is less significant with VGG16 backbone than with ResNet101 backbone. This is probably because that the semantic segmentation using VGG16 is not as accurate as using ResNet101 on the source domain, leading to affinity space to be aligned far from the ground-truth affinity space. This makes the adaptation more challenging.

It is noteworthy that most methods do not perform well on the under-represented classes (e.g., fence, pole and light) shown in Tab. I and Tab. II. This is a common class imbalance issue in unsupervised domain adaptation. During adaptation, the network tends to pay more attention to the dominated classes than other classes. Consequently, the proposed method brings consistent performance improvements on the high frequent classes (e.g., road, building and sky) but not on the infrequent classes (e.g., fence, pole and light). Despite this, as depicted in Tab. I and Tab. II, the overall performance is still very encouraging. It is likely that combining with class balanced techniques may achieve better performances, which is a promising direction to be explored in the future.

Complementary with IT and ST. Most recent works aim to solve the UDA semantic segmentation problem by leveraging the following three strategies: 1) image translation (IT) that bridges up the image style differences; 2) distribution alignment (DA) which aims to align distribution of intermediate feature or output prediction; 3) self-training that effectively uses pseudo labels. As demonstrated in [49], [50], these

TABLE III
COMPLEMENTARY OF THE PROPOSED ASA RELYING ON DISTRIBUTION ALIGNMENT (DA) WITH IMAGE TRANSLATION (IT) AND SELF-TRAINING (ST).

(a) GTA5 → Cityscapes				
Method	IT	DA	ST	mIOU
DCAN [47]	✓	✓		41.7
CBST [48]			✓	41.5
DISE [49]	✓	✓		45.4
SODPR [44]	✓	✓	✓	46.5
BDL [50]	✓	✓	✓	48.5
ASA (our)		✓		45.1
ASA + IT (our)	✓	✓		45.6
ASA + ST (our)		✓	✓	48.1
ASA + IT + ST (our)	✓	✓	✓	49.1
(b) SYNTHIA → Cityscapes				
Method	IT	DA	ST	mIOU
DCAN [47]	✓	✓		44.9
CBST [48]			✓	36.9
DISE [49]	✓	✓		48.8
SODPR [44]	✓	✓	✓	46.5
BDL [50]	✓	✓	✓	51.4
ASA (our)		✓		49.3
ASA + IT (our)	✓	✓		49.8
ASA + ST (our)		✓	✓	52.4
ASA + IT + ST (our)	✓	✓	✓	53.8

three strategies are complementary to each other. Though the proposed method mainly focuses on distribution alignment (DA) of output prediction, we also discuss the complementary of the proposed ASA with IT and ST technique.

Image translation is an intuitive way to reduce the domain gap on image level in unsupervised domain adaptation. We first explore the complementary with IT by utilizing CyCADA [10] to generate target-like images from source domain images. Then, we perform adaptation with ASA from new generated images to target images. Since domain gap has been somehow reduced by image translation, the weight of ASA adaptation

TABLE IV
SENSITIVITY ANALYSIS OF LOSS WEIGHT λ FOR ASC AND ASA.

GTA5 \rightarrow Cityscapes					
λ	0.0002	0.0005	0.001	0.002	0.004
λ_{ASC}	43.1	43.5	43.8	43.6	43.7
λ_{ASA}	44.9	45.0	45.1	44.7	44.6

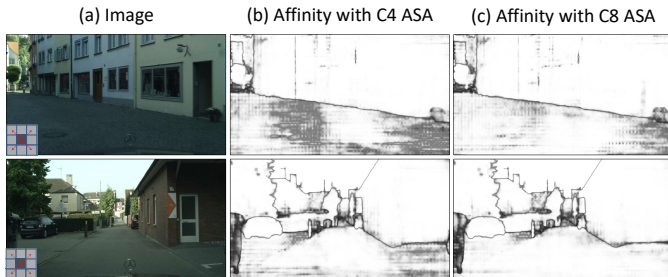


Fig. 4. Diagonal affinity visualization for ASA with different connectivity settings on GTA5 \rightarrow Cityscapes adaptation on some target images in (a). (b) and (c) show the diagonal affinity given by the average Cosine similarity between predictions of each pixel and all its diagonal neighboring pixels for ASA under 4-connectivity (C4) and 8-connectivity (C8) setting, respectively.

λ_{ASA} in Eq. (6) is set to 0.0001 in this experiment. As depicted in Tab. III, the image translation technique brings performance gain to the proposed approach on both GTA5 \rightarrow Cityscapes and SYNTHIA \rightarrow Cityscapes adaptation, revealing that image translation is complementary to the proposed ASA adaptation.

Self-training is another common strategy in unsupervised domain adaptation. The core of self-training is how to get “correct” pseudo labels. We take the model adapted with the proposed ASA to generate pseudo labels in a straightforward way. Specifically, for each pixel x in an image, we verify the Softmax output on that pixel. If the highest confidence is larger than 0.9, we consider the predicted class as the pseudo label on x . Otherwise, we simply set it to *ignored* label, which will be ignored in gradient back-propagation. We re-train the segmentation network with such pseudo labels on target domain. As shown in Tab. III, the proposed approach is also complementary to the self-training strategy. More specifically, on GTA5 \rightarrow Cityscapes adaptation, the proposed ASA combined with self-training strategy yields 48.1% mIoU, performing similarly with BDL [50] which relies on extra image translation strategy. On SYNTHIA \rightarrow Cityscapes adaptation, the proposed ASA combined with self-training strategy achieves 52.4% mIoU, improving BDL [50] by 1.0% mIoU.

Image translation and self-training may further be complementary to distribution alignment based methods [50], [44]. For a fair comparison with BDL [50] and SODPR [44], we also equip the proposed ASA with both image translation and self-training strategies to further boost performance. As depicted in Tab. III, we achieve the state-of-the-art performance on both GTA5 \rightarrow Cityscapes and SYNTHIA \rightarrow Cityscapes benchmarks, which further demonstrates the complementarity of ASA to image translation and self-training. Specifically, we get 49.1% mIoU on GTA5 \rightarrow Cityscapes adaptation, outperforming BDL [50] by 0.6% mIoU and SODPR [44] by 2.6%

TABLE V
ABLATION STUDY ON THE NUMBER OF ADJACENT PIXELS N INVOLVED IN THE PROPOSED CONCEPT OF AFFINITY SPACE AND MODEL COMPLEXITY ANALYSIS ON GTA5 \rightarrow CITYSCAPES ADAPTATION.

Method	Connectivity (N)	GFLOPs	Memory(M)	mIoU
Baseline	-	644.9	9340	38.1
AdaptSegNet [14]	-	1087.8	9602	41.4
ASC	4	1041.7	9528	42.6
	8	1042.3	9532	43.8
ASA	4	1129.3	9628	43.6
	8	1167.7	9654	45.1

mIoU, respectively. On SYNTHIA \rightarrow Cityscapes adaptation, we achieve 53.8 % mIoU, which improves BDL [50] by 2.4% mIoU and SODPR [44] by 7.3 % mIoU, respectively.

D. Ablation Study

We conduct ablation study on two major components of the proposed method: 1) loss weight hyper-parameters λ_{ASC} in Eq. (3) and λ_{ASA} in Eq. (6); 2) Different connectivity in defining the affinity space.

Ablation study on hyper-parameters. The weighting factor λ_{ASC} for ASC and λ_{ASA} for ASA are two important hyper-parameters. We adopt a sensitivity analysis on these two hyper-parameters. We evaluate the performance of both ASC and ASA with different weighting factors on GTA5 \rightarrow Cityscapes adaptation. As depicted in Tab. IV, both ASC and ASA can tolerate a large range of weighting factors. And we set both λ_{ASC} and λ_{ASA} to 0.001 in all experiments.

Ablation study on different connectivity. We also study the effect of different connectivity settings involved in defining the affinity space. For that, we conduct experiments with 4-connectivity and 8-connectivity on the GTA5 \rightarrow Cityscapes adaptation. As depicted in Tab. V, both ASC and ASA strategies for affinity space adaptation achieve better performance with 8-connectivity, showing that the co-occurring patterns revealing the output structure is important for unsupervised domain adaptation in semantic segmentation. To further understand the impact of different connectivity, we also visualize the diagonal affinity maps for ASA with different connectivity settings on GTA5 \rightarrow Cityscapes adaptation on some target images. As shown in Fig. 4, for each pixel, we calculate the average Cosine similarity with its 4 diagonal neighbors (see red arrows on the bottom left of target images in Fig. 4). It can be observed that ASA with 8-connectivity (C8) setting achieves better diagonal affinity than ASA under 4-connectivity (C4) setting, which leads to better segmentation performance.

E. Model complexity analysis

We also analyze the amount of computation and memory footprint during training. The extra computational complexity of both ASC and ASA is $\mathcal{O}(N \times H \times W)$, where $H \times W$ donates the spatial resolution of output prediction and N denotes the number of involved adjacent pixels. As shown in Tab. V, compared with AdaptSegNet [14], both the proposed

TABLE VI
QUANTITATIVE COMPARISON WITH SOME STATE-OF-THE-ART METHODS ON ADAPTING CITYSCAPES TO CROSS-CITY DATASET.

		Cityscapes → Cross-City													
City	Method	road	sidewalk	building	light	sign	veg	sky	person	rider	car	bus	mbike	bike	mIoU
Rome	Cross-City [62]	79.5	29.3	84.5	0.0	22.2	80.6	82.8	29.5	13.0	71.7	37.5	25.9	1.0	42.9
	CBST [48]	87.1	43.9	89.7	14.8	47.7	85.4	90.3	45.4	26.6	85.4	20.5	49.8	10.3	53.6
	AdaptSegNet [14]	83.9	34.2	88.3	18.8	40.2	86.2	93.1	47.8	21.7	80.9	47.8	48.3	8.6	53.8
	MaxSquare [43]	80.0	27.6	87.0	20.8	42.5	85.1	92.4	46.7	22.9	82.1	53.5	50.8	8.8	53.9
	Source Only (our)	83.8	37.1	87.1	15.7	39.6	84.4	92.2	30.5	20.5	80.3	47.4	38.5	2.8	50.8
	ASA (our)	84.9	35.1	87.5	17.3	40.3	85.3	92.3	47.0	25.2	81.7	49.7	49.3	8.7	54.2
Rio	Cross-City [62]	74.2	43.9	79.0	2.4	7.5	77.8	69.5	39.3	10.3	67.9	41.2	27.9	10.9	42.5
	CBST [48]	84.3	55.2	85.4	19.6	30.1	80.5	77.9	55.2	28.6	79.7	33.2	37.6	11.5	52.2
	AdaptSegNet [14]	76.2	44.7	84.6	9.3	25.5	81.8	87.3	55.3	32.7	74.3	28.9	43.0	27.6	51.6
	MaxSquare [43]	70.9	39.2	85.6	14.5	19.7	81.8	88.1	55.2	31.5	77.2	39.3	43.1	30.1	52.0
	Source Only (our)	76.4	50.3	81.8	14.8	16.8	77.5	86.1	36.1	17.6	76.9	45.1	28.3	12.7	47.7
	ASA (our)	79.1	49.8	84.9	14.3	20.8	80.2	87.6	54.9	33.7	78.3	40.0	50.9	32.0	54.4
Tokyo	Cross-City [62]	83.4	35.4	72.8	12.3	12.7	77.4	64.3	42.7	21.5	64.1	20.8	8.9	40.3	42.8
	CBST [48]	85.2	33.6	80.4	8.3	31.1	83.9	78.2	53.2	28.9	72.7	4.4	27.0	47.0	48.8
	AdaptSegNet [14]	81.5	26.0	77.8	17.8	26.8	82.7	90.9	55.8	38.0	72.1	4.2	24.5	50.8	49.9
	MaxSquare [43]	79.3	28.5	78.3	14.5	27.9	82.8	89.6	57.3	31.9	71.9	6.0	29.1	49.2	49.7
	Source Only (our)	82.8	34.4	76.0	15.9	24.7	79.2	87.3	41.4	31.7	70.9	5.1	87.3	24.7	46.8
	ASA (our)	83.2	29.1	77.8	16.6	27.2	82.6	89.5	56.2	33.9	72.7	6.0	30.4	49.8	50.4
Taipei	Cross-City [62]	78.6	28.6	80.0	13.1	7.6	68.2	82.1	16.8	9.4	60.4	34.0	26.5	9.9	39.6
	CBST [48]	86.1	35.2	84.2	15.0	22.2	75.6	74.9	22.7	33.1	78.0	37.6	58.0	30.9	50.3
	AdaptSegNet [14]	81.7	29.5	85.2	26.4	15.6	76.7	91.7	31.0	12.5	71.5	41.1	47.3	27.7	49.1
	MaxSquare [43]	81.2	32.8	85.4	31.9	14.7	78.3	92.7	28.3	8.6	68.2	42.2	51.3	32.4	49.8
	Source Only (our)	82.9	33.4	86.1	22.7	15.1	76.4	92.2	15.1	17.2	70.9	38.7	48.9	17.4	47.5
	ASA (our)	82.6	30.8	86.3	26.0	15.1	77.0	92.3	28.4	9.1	71.9	39.8	47.4	31.0	49.1

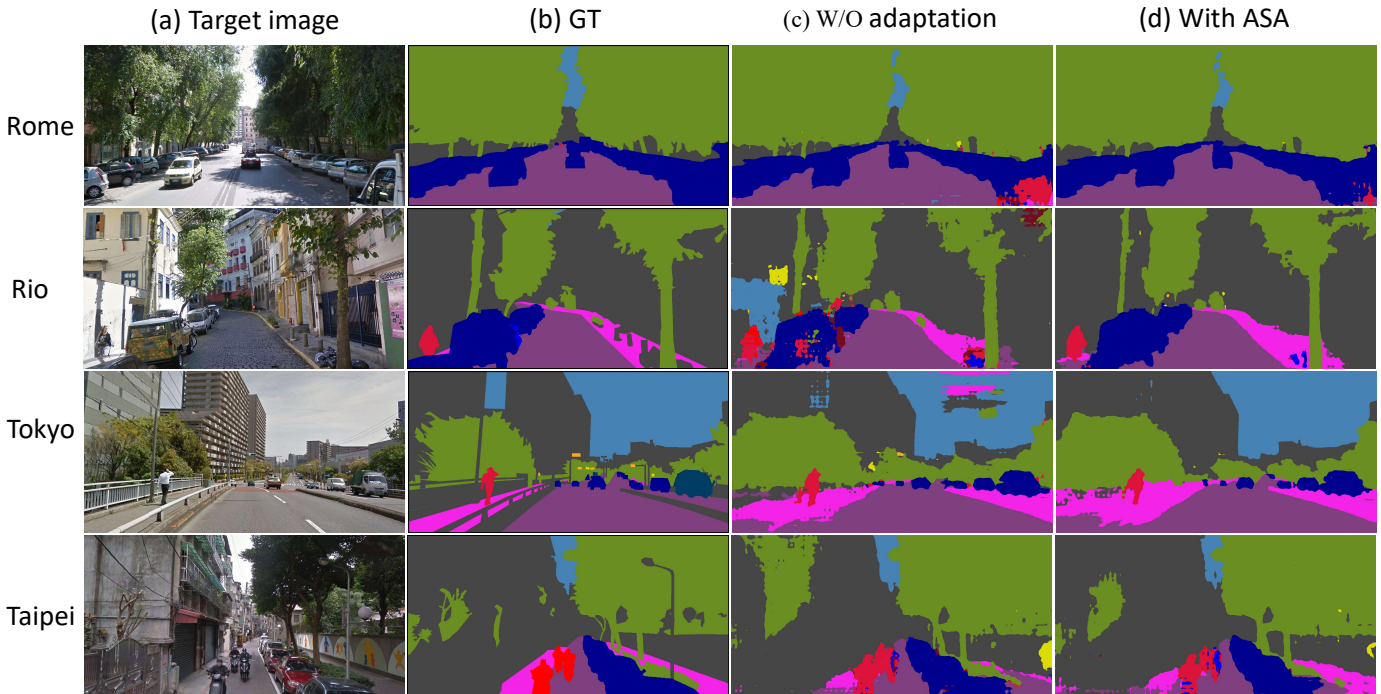


Fig. 5. Some qualitative results on Cityscapes → Cross-city adaptation. From left to right: (a) target image; (b) ground-truth segmentation; (c) segmentation without adaptation; (d) segmentation with affinity space alignment (ASA) adaptation.

TABLE VII

QUANTITATIVE RESULTS IN TERMS OF DICE COEFFICIENT FOR ADAPTING REFUGE TO RIM-ONE-R3 ON ‘TEST’ SPLIT OF RIM-ONE-R3.

Method	RIM-ONE-r3		
	$Dice_{cup}$	$Dice_{disc}$	Mean
Source only	0.751	0.793	0.772
Oracle	0.856	0.968	0.914
AdaptSegNet [14]	0.775	0.893	0.834
ASA (ours)	0.806	0.900	0.853

ASC and ASA achieve better performance while slightly increasing the computation cost and memory usage during training.

F. Real-to-Real adaptation results

Based on the synthetic-to-real adaptation evaluation, the proposed ASA strategy is in general more effective than the proposed ASC strategy for affinity space adaptation. We evaluate the proposed ASA on two real-to-real segmentation adaptations to further demonstrate the effectiveness of the proposed method.

Cross-City → Cityscapes. Most existing works for UDA semantic segmentation mainly focus on synthetic-to-real situation, especially on synthetic-to-cityscapes task. In practice, domain shift across different cities is a more realistic and challenging scenario. To verify the effectiveness of the proposed method on real-to-real adaptation, we conduct experiments on adapting semantic segmentation from Cityscapes dataset to Cross-city dataset. We list our baseline and ASA results in Tab. VI, and compare with some other state-of-the-art methods. As shown in Tab. VI, for small domain gap in real-to-real scenario, the proposed approach also achieves consistent improvement for different cities. Some qualitative segmentation results are illustrated in Fig. 5. The proposed ASA effectively improves the segmentation results without any adaptation.

REFUGE → RIM-ONE-r3. In addition to urban scene adaptation, the domain gap is also an important issue in medical image analysis. To verify the generalizability of the proposed approach, we conduct an experiment on unsupervised domain adaptation for retinal optic disk and cup segmentation. Specifically, we adopt Deeplabv3-plus [16] as the baseline, and evaluate the most related AdaptSegNet [14] and the proposed ASA using the same experimental settings. As shown in Tab. VII. The proposed ASA consistently outperforms the baseline and AdaptSegNet [14]. Some qualitative results are illustrated in Fig. 6. The proposed ASA effectively bridges up the domain gap between the source and target domains.

G. Weakness

As demonstrated in previous experimental results, the proposed method performs well in most situations. However, it stills fails to handle some difficult problems, such as delicate structure, region inconsistency. The proposed method also

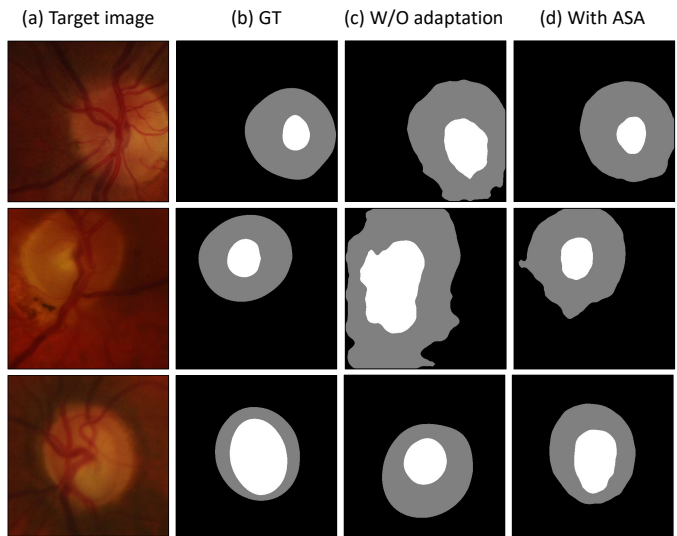


Fig. 6. Some qualitative results on REFUGE → RIM-ONE-r3 adaptation.

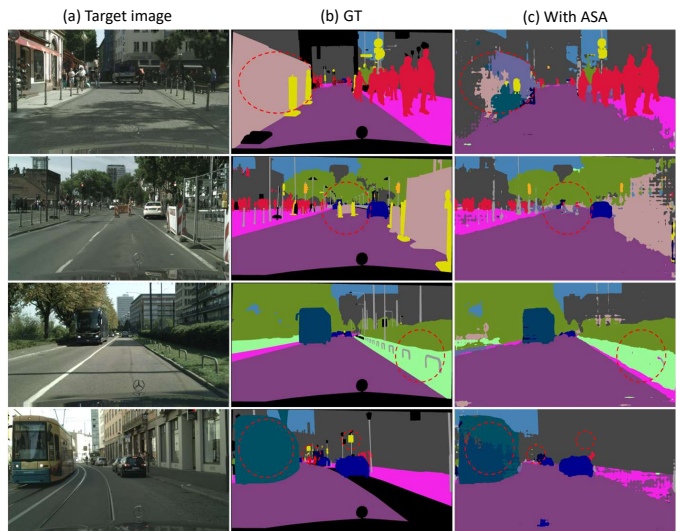


Fig. 7. Some failure examples (see the region enclosed by red circles) from GTA5 → Cityscapes adaptation.

works less well for lower frequent classes (e.g., light and pole). Some failure cases are shown in Fig. 7. Note that these difficult problems are also challenging for the other state-of-the-art methods.

V. CONCLUSION

In this paper, we address the problem of unsupervised domain adaptation for semantic segmentation. Considering that the output of semantic segmentation is usually structured and has invariant structures across domains, we propose to leverage such invariance through exploiting affinity relationship between adjacent pixels in the output level instead of adapting domains on individual per-pixel information for most state-of-the-art methods. To this end, we introduce the concept of affinity space encoding the affinity relationship. We exploit two affinity space adaptation strategies: affinity space cleaning and adversarial affinity space alignment. Both affinity space

adaptation schemes effectively align the co-occurring patterns that reveal the output structure of semantic segmentation of source and target domain, leading to superior performance over some state-of-the-art methods. This demonstrates for the first time that the affinity relationship is beneficial for unsupervised domain adaptation in semantic segmentation. In the future, we plan to investigate the combination of the two proposed affinity space adaptation strategies and combine the proposed output level adaptation with other adaptations on image and/or feature level. We would also like to explore the complementarity of the proposed method with recent class- or region-conditioned adaptation to further boost the performance.

ACKNOWLEDGMENT

This work was supported in part by the Major Project for New Generation of AI under Grant no. 2018AAA0100400, NSFC 61703171, and NSF of Hubei Province of China under Grant 2018CFB199. Dr. Yongchao Xu was supported by the Young Elite Scientists Sponsorship Program by CAST.

REFERENCES

- [1] J. Long, E. Shelhamer, and T. Darrell, "Fully convolutional networks for semantic segmentation," in *Proc. of IEEE Intl. Conf. on Computer Vision and Pattern Recognition*, 2015, pp. 3431–3440.
- [2] S. Zheng, S. Jayasumana, B. Romera-Paredes, V. Vineet, Z. Su, D. Du, C. Huang, and P. H. Torr, "Conditional random fields as recurrent neural networks," in *Proc. of IEEE Intl. Conf. on Computer Vision and Pattern Recognition*, 2015, pp. 1529–1537.
- [3] H. Zhao, J. Shi, X. Qi, X. Wang, and J. Jia, "Pyramid scene parsing network," in *Proc. of IEEE Intl. Conf. on Computer Vision and Pattern Recognition*, 2017, pp. 2881–2890.
- [4] L.-C. Chen, G. Papandreou, I. Kokkinos, K. Murphy, and A. L. Yuille, "DeepLab: Semantic image segmentation with deep convolutional nets, atrous convolution, and fully connected crfs," *IEEE Trans. Pattern Anal. Mach. Intell.*, vol. 40, no. 4, pp. 834–848, 2018.
- [5] H. Zhang, K. Dana, J. Shi, Z. Zhang, X. Wang, A. Tyagi, and A. Agrawal, "Context encoding for semantic segmentation," in *Proc. of IEEE Intl. Conf. on Computer Vision and Pattern Recognition*, 2018, pp. 7151–7160.
- [6] H. Zhao, Y. Zhang, S. Liu, J. Shi, C. Change Loy, D. Lin, and J. Jia, "Psanet: Point-wise spatial attention network for scene parsing," in *Proc. of European Conference on Computer Vision*, 2018, pp. 267–283.
- [7] T.-W. Ke, J.-J. Hwang, Z. Liu, and S. X. Yu, "Adaptive affinity fields for semantic segmentation," in *Proc. of European Conference on Computer Vision*, 2018, pp. 587–602.
- [8] M. Zhen, J. Wang, L. Zhou, T. Fang, and L. Quan, "Learning fully dense neural networks for image semantic segmentation," in *Proc. of the AAAI Conf. on Artificial Intelligence*, 2019.
- [9] I. Goodfellow, J. Pouget-Abadie, M. Mirza, B. Xu, D. Warde-Farley, S. Ozair, A. Courville, and Y. Bengio, "Generative adversarial nets," in *Proc. of Advances in Neural Information Processing Systems*, 2014, pp. 2672–2680.
- [10] J. Hoffman, E. Tzeng, T. Park, a. P. I. Jun-Yan Zhu, K. Saenko, A. A. Efros, and T. Darrell, "Cycada: Cycle consistent adversarial domain adaptation," in *Proc. of Intl. Conf. on Machine Learning*, 2018, pp. 1994–2003.
- [11] J. Hoffman, D. Wang, F. Yu, and T. Darrell, "FCNs in the wild: Pixel-level adversarial and constraint-based adaptation," *arXiv preprint arXiv:1612.02649*, 2016.
- [12] S. Sankaranarayanan, Y. Balaji, A. Jain, S. Nam Lim, and R. Chellappa, "Learning from synthetic data: Addressing domain shift for semantic segmentation," in *Proc. of IEEE Intl. Conf. on Computer Vision and Pattern Recognition*, 2018, pp. 3752–3761.
- [13] Y. Zhang, Z. Qiu, T. Yao, D. Liu, and T. Mei, "Fully convolutional adaptation networks for semantic segmentation," in *Proc. of IEEE Intl. Conf. on Computer Vision and Pattern Recognition*, 2018, pp. 6810–6818.
- [14] Y.-H. Tsai, W.-C. Hung, S. Schuler, K. Sohn, M.-H. Yang, and M. Chandraker, "Learning to adapt structured output space for semantic segmentation," in *Proc. of IEEE Intl. Conf. on Computer Vision and Pattern Recognition*, 2018, pp. 7472–7481.
- [15] O. Ronneberger, P. Fischer, and T. Brox, "U-net: Convolutional networks for biomedical image segmentation," in *Proc. of Intl. Conf. on Medical Image Computing and Computer Assisted Intervention*, vol. 9351, 2015, pp. 234–241.
- [16] L.-C. Chen, Y. Zhu, G. Papandreou, F. Schroff, and H. Adam, "Encoder-decoder with atrous separable convolution for semantic image segmentation," in *Proc. of European Conference on Computer Vision*, 2018, pp. 801–818.
- [17] S. Liu, S. De Mello, J. Gu, G. Zhong, M.-H. Yang, and J. Kautz, "Learning affinity via spatial propagation networks," in *Proc. of Advances in Neural Information Processing Systems*, 2017, pp. 1520–1530.
- [18] J. Fu, J. Liu, H. Tian, Y. Li, Y. Bao, Z. Fang, and H. Lu, "Dual attention network for scene segmentation," in *Proc. of IEEE Intl. Conf. on Computer Vision and Pattern Recognition*, 2019, pp. 3146–3154.
- [19] Y. Yuan and J. Wang, "Ocnet: Object context network for scene parsing," *arXiv preprint arXiv:1809.00916*, 2018.
- [20] S. R. Richter, V. Vineet, S. Roth, and V. Koltun, "Playing for data: Ground truth from computer games," in *Proc. of European Conference on Computer Vision*, vol. 9906, 2016, pp. 102–118.
- [21] Z. Huang, X. Wang, J. Wang, W. Liu, and J. Wang, "Weakly-supervised semantic segmentation network with deep seeded region growing," in *Proc. of IEEE Intl. Conf. on Computer Vision and Pattern Recognition*, 2018, pp. 7014–7023.
- [22] X. Li, H. Ma, and X. Luo, "Weakly supervised semantic segmentation with only one image level annotation per category," *IEEE Trans. on Image Processing*, vol. 29, pp. 128–141, 2019.
- [23] J. Dai, K. He, and J. Sun, "Boxsup: Exploiting bounding boxes to supervise convolutional networks for semantic segmentation," in *Proc. of IEEE Intl. Conf. on Computer Vision*, 2015, pp. 1635–1643.
- [24] A. Khoreva, R. Benenson, J. Hosang, M. Hein, and B. Schiele, "Simple does it: Weakly supervised instance and semantic segmentation," in *Proc. of IEEE Intl. Conf. on Computer Vision and Pattern Recognition*, 2017, pp. 876–885.
- [25] D. Lin, J. Dai, J. Jia, K. He, and J. Sun, "Scribblesup: Scribble-supervised convolutional networks for semantic segmentation," in *Proc. of IEEE Intl. Conf. on Computer Vision and Pattern Recognition*, 2016, pp. 3159–3167.
- [26] G. Ros, L. Sellart, J. Materzynska, D. Vazquez, and A. M. Lopez, "The synthia dataset: A large collection of synthetic images for semantic segmentation of urban scenes," in *Proc. of IEEE Intl. Conf. on Computer Vision and Pattern Recognition*, 2016, pp. 3234–3243.
- [27] T. Poggio, "Early vision: From computational structure to algorithms and parallel hardware," in *Human and Machine Vision II*. Elsevier, 1986, pp. 190–206.
- [28] J. Shi and M. Jitendra, "Normalized cuts and image segmentation," *IEEE Trans. Pattern Anal. Mach. Intell.*, vol. 22, no. 8, pp. 888–905, 2000.
- [29] X. Wang, Y. Tang, S. Masnou, and L. Chen, "A global/local affinity graph for image segmentation," *IEEE Trans. on Image Processing*, vol. 24, no. 4, pp. 1399–1411, 2015.
- [30] Y. Liu, S. Yang, B. Li, W. Zhou, J. Xu, H. Li, and Y. Lu, "Affinity derivation and graph merge for instance segmentation," in *Proc. of European Conference on Computer Vision*, 2018, pp. 686–703.
- [31] E. Tzeng, J. Hoffman, K. Saenko, and T. Darrell, "Adversarial discriminative domain adaptation," in *Proc. of IEEE Intl. Conf. on Computer Vision and Pattern Recognition*, 2017, pp. 7167–7176.
- [32] W. Zhang, W. Ouyang, W. Li, and D. Xu, "Collaborative and adversarial network for unsupervised domain adaptation," in *Proc. of IEEE Intl. Conf. on Computer Vision and Pattern Recognition*, 2018, pp. 3801–3809.
- [33] K. Saito, K. Watanabe, Y. Ushiku, and T. Harada, "Maximum classifier discrepancy for unsupervised domain adaptation," in *Proc. of IEEE Intl. Conf. on Computer Vision*, 2018, pp. 3723–3732.
- [34] S. Xie, Z. Zheng, L. Chen, and C. Chen, "Learning semantic representations for unsupervised domain adaptation," in *Proc. of Intl. Conf. on Machine Learning*, 2018, pp. 5419–5428.
- [35] M. Long, H. Zhu, J. Wang, and M. I. Jordan, "Unsupervised domain adaptation with residual transfer networks," in *Proc. of Advances in Neural Information Processing Systems*, 2016, pp. 136–144.
- [36] K. Saito, Y. Ushiku, T. Harada, and K. Saenko, "Adversarial dropout regularization," in *Proc. of International Conference on Learning Representations*, 2017.

- [37] S. Li, S. Song, G. Huang, Z. Ding, and C. Wu, "Domain invariant and class discriminative feature learning for visual domain adaptation," *IEEE Trans. on Image Processing*, vol. 27, no. 9, pp. 4260–4273, 2018.
- [38] J. Li, M. Jing, K. Lu, L. Zhu, and H. T. Shen, "Locality preserving joint transfer for domain adaptation," *IEEE Trans. on Image Processing*, vol. 28, no. 12, pp. 6103–6115, 2019.
- [39] W. Hong, Z. Wang, M. Yang, and J. Yuan, "Conditional generative adversarial network for structured domain adaptation," in *Proc. of IEEE Intl. Conf. on Computer Vision and Pattern Recognition*, 2018, pp. 1335–1344.
- [40] Q. Wang, J. Gao, and X. Li, "Weakly supervised adversarial domain adaptation for semantic segmentation in urban scenes," *IEEE Trans. on Image Processing*, vol. 28, no. 9, pp. 4376–4386, 2019.
- [41] Y. Luo, P. Liu, T. Guan, J. Yu, and Y. Yang, "Significance-aware information bottleneck for domain adaptive semantic segmentation," in *Proc. of IEEE Intl. Conf. on Computer Vision*, October 2019.
- [42] T.-H. Vu, H. Jain, M. Bucher, M. Cord, and P. Pérez, "Advent: Adversarial entropy minimization for domain adaptation in semantic segmentation," in *Proc. of IEEE Intl. Conf. on Computer Vision and Pattern Recognition*, 2019, pp. 2517–2526.
- [43] M. Chen, H. Xue, and D. Cai, "Domain adaptation for semantic segmentation with maximum squares loss," in *Proc. of IEEE Intl. Conf. on Computer Vision*, 2019, pp. 2090–2099.
- [44] Y.-H. Tsai, K. Sohn, S. Schuler, and M. Chandraker, "Domain adaptation for structured output via discriminative patch representations," in *Proc. of IEEE Intl. Conf. on Computer Vision*, 2019.
- [45] Y. Luo, L. Zheng, T. Guan, J. Yu, and Y. Yang, "Taking a closer look at domain shift: Category-level adversaries for semantics consistent domain adaptation," in *Proc. of IEEE Intl. Conf. on Computer Vision and Pattern Recognition*, 2019, pp. 2507–2516.
- [46] L. Du, J. Tan, H. Yang, J. Feng, X. Xue, Q. Zheng, X. Ye, and X. Zhang, "Ssf-dan: Separated semantic feature based domain adaptation network for semantic segmentation," in *Proc. of IEEE Intl. Conf. on Computer Vision*, 2019, pp. 982–991.
- [47] Z. Wu, X. Han, Y.-L. Lin, M. Gokhan Uzunbas, T. Goldstein, S. Nam Lim, and L. S. Davis, "DCAN: Dual channel-wise alignment networks for unsupervised scene adaptation," in *Proc. of European Conference on Computer Vision*, 2018, pp. 518–534.
- [48] Y. Zou, Z. Yu, B. Vijaya Kumar, and J. Wang, "Unsupervised domain adaptation for semantic segmentation via class-balanced self-training," in *Proc. of European Conference on Computer Vision*, 2018, pp. 289–305.
- [49] W.-L. Chang, H.-P. Wang, W.-H. Peng, and W.-C. Chiu, "All about structure: Adapting structural information across domains for boosting semantic segmentation," in *Proc. of IEEE Intl. Conf. on Computer Vision and Pattern Recognition*, 2019, pp. 1900–1909.
- [50] Y. Li, L. Yuan, and N. Vasconcelos, "Bidirectional learning for domain adaptation of semantic segmentation," in *Proc. of IEEE Intl. Conf. on Computer Vision and Pattern Recognition*, 2019, pp. 6936–6945.
- [51] J.-Y. Zhu, T. Park, P. Isola, and A. A. Efros, "Unpaired image-to-image translation using cycle-consistent adversarial networks," in *Proc. of IEEE Intl. Conf. on Computer Vision*, 2017, pp. 2223–2232.
- [52] F. Sadat Saleh, M. Sadegh Aliakbarian, M. Salzmänn, L. Petersson, and J. M. Alvarez, "Effective use of synthetic data for urban scene semantic segmentation," in *Proc. of European Conference on Computer Vision*, 2018, pp. 84–100.
- [53] X. Zhu, H. Zhou, C. Yang, J. Shi, and D. Lin, "Penalizing top performers: Conservative loss for semantic segmentation adaptation," in *Proc. of European Conference on Computer Vision*, 2018, pp. 568–583.
- [54] C. Sakaridis, D. Dai, S. Hecker, and L. Van Gool, "Model adaptation with synthetic and real data for semantic dense foggy scene understanding," in *Proc. of European Conference on Computer Vision*, 2018, pp. 687–704.
- [55] C. Sakaridis, D. Dai, and L. Van Gool, "Semantic foggy scene understanding with synthetic data," *International Journal of Computer Vision*, vol. 126, no. 9, pp. 973–992, 2018.
- [56] Y. Xu, B. Du, L. Zhang, Q. Zhang, G. Wang, and L. Zhang, "Self-ensembling attention networks: Addressing domain shift for semantic segmentation," in *Proc. of the AAAI Conf. on Artificial Intelligence*, vol. 33, 2019, pp. 5581–5588.
- [57] J. Choi, T. Kim, and C. Kim, "Self-ensembling with gan-based data augmentation for domain adaptation in semantic segmentation," in *Proc. of IEEE Intl. Conf. on Computer Vision*, 2019, pp. 6830–6840.
- [58] K. Simonyan and A. Zisserman, "Very deep convolutional networks for large-scale image recognition," in *Proc. of International Conference on Learning Representations*, 2015.
- [59] K. He, X. Zhang, S. Ren, and J. Sun, "Deep residual learning for image recognition," in *Proc. of IEEE Intl. Conf. on Computer Vision and Pattern Recognition*, 2016, pp. 770–778.
- [60] O. Russakovsky, J. Deng, H. Su, J. Krause, S. Satheesh, S. Ma, Z. Huang, A. Karpathy, A. Khosla, M. Bernstein *et al.*, "Imagenet large scale visual recognition challenge," *International Journal of Computer Vision*, vol. 115, no. 3, pp. 211–252, 2015.
- [61] M. Cordts, M. Omran, S. Ramos, T. Rehfeld, M. Enzweiler, R. Benenson, U. Franke, S. Roth, and B. Schiele, "The cityscapes dataset for semantic urban scene understanding," in *Proc. of IEEE Intl. Conf. on Computer Vision and Pattern Recognition*, 2016, pp. 3213–3223.
- [62] Y.-H. Chen, W.-Y. Chen, Y.-T. Chen, B.-C. Tsai, Y.-C. Frank Wang, and M. Sun, "No more discrimination: Cross city adaptation of road scene segmenters," in *Proc. of IEEE Intl. Conf. on Computer Vision*, 2017, pp. 1992–2001.
- [63] J. I. Orlando, H. Fu, J. B. Breda, K. van Keer, D. R. Bathula, A. Diaz-Pinto, R. Fang, P.-A. Heng, J. Kim, J. Lee *et al.*, "Refuge challenge: A unified framework for evaluating automated methods for glaucoma assessment from fundus photographs," *Medical image analysis*, vol. 59, p. 101570, 2020.
- [64] F. Fumero, S. Alayón, J. L. Sanchez, J. Sigut, and M. Gonzalez-Hernandez, "Rim-one: An open retinal image database for optic nerve evaluation," in *CBMS. IEEE*, 2011, pp. 1–6.
- [65] A. Paszke, S. Gross, S. Chintala, G. Chanan, E. Yang, Z. DeVito, Z. Lin, A. Desmaison, L. Antiga, and A. Lerer, "Automatic differentiation in pytorch," in *NIPS workshop*, 2017.